Energy Reports 9 (2023) 873–885

Contents lists available at ScienceDirect

Energy Reports

journal homepage: www.elsevier.com/locate/egyr

Research paper

Dynamic downscaling of wind speed over the North Atlantic Ocean using CMIP6 projections: Implications for offshore wind power density

José C. Fernández-Alvarez [a,b,*], Xurxo Costoya [a], Albenis Pérez-Alarcón [a,b], Stefan Rahimi [c], Raquel Nieto [a], Luis Gimeno [a]

[a] Centro de Investigación Mariña, Universidade de Vigo, Environmental Physics Laboratory (EPhysLab), Campus As Lagoas s/n, Ourense, 32004, Spain
[b] Departamento de Meteorología, Instituto Superior de Tecnologías y Ciencias Aplicadas, Universidad de La Habana, La Habana, Cuba
[c] Department of Atmospheric and Oceanic Sciences, University of California, Los Angeles, United States

ARTICLE INFO

Article history:
Received 22 July 2022
Received in revised form 7 November 2022
Accepted 11 December 2022
Available online xxxx

Dataset link: https://cds.climate.copernicus.eu/cdsapp#!/dataset/reanalysis-era5-single-levels-monthly-means?tab=form, https://esgf-data.dkrz.de/search/cmip6-dkrz/

Keywords:
Wind power density (WPD)
Dynamic downscaling
WRF-ARW model
CMIP6
Climate change

ABSTRACT

Offshore wind energy is an important agent to fight climate change. However, it is simultaneously very sensitive to climate change. This study analyzes the future changes in wind speed of 10 m above sea surface (V10) in the North Atlantic Ocean and how these variations may affect offshore wind energy resources for three potential subregions (the United States (US) East Coast, western Iberian Peninsula, and the Caribbean Sea). Dynamic downscaling of three different future scenarios of the CESM2 global climate model (CMIP6 project) was performed using the WRF-ARW atmospheric model. V10 is expected to decrease in the winter and spring seasons but increase in summer and autumn, mainly in tropical regions up to 30 °N. Annually, it shows the maximum increase in the tropical region. For the Iberian Peninsula subregion, significant increases in summer are expected for wind power density (WPD) along the 21st century, but there is uncertainty for the other seasons. A WPD decrease in winter and increases in summer and autumn are expected along the 21st century for the US subregion. No significant changes were observed at annual scale. Finally, for the Caribbean Sea, a decrease is projected in the Yucatan Basin and considerable increases are foreseen for the Colombia and Venezuela basins.

1. Introduction

Climate change presents a real challenge to society. According to the sixth report of the Intergovernmental Panel on Climate Change (IPCC), an increase in global surface temperature of 1.5 °C and 2 °C will be exceeded during the 21st century unless significant reductions in CO_2 and other greenhouse gas emissions are achieved in the coming decades (IPCC, 2021). Although temperature has received the most attention in relation to climate change, it is important to analyse other atmospheric variables that are instrumental for the climate system. One of these variables is wind speed of 10 m above sea surface (V10). V10 is a key variable in climate studies because its variations have substantial impacts on human society and the natural environment (Pryor et al., 2006). For example, V10 intensification can exacerbate soil erosion, leading to more severe dust storms (Alizadeh-Choobari et al., 2014; Wang et al., 2017) and result in heat and humidity fluxes at the air–sea interface (Renault et al., 2017).

Renewable energy sources are important alternatives to alleviate the dependence on fossil fuels and reduce greenhouse gas emissions. Offshore wind energy is a mature marine renewable energy source that still has high growth potential owing to technological advances, such as floating structures that allow the installation of offshore wind farms at greater depths. Although an increase in the offshore wind installation capacity is expected worldwide (GWEC, 2021), it is important to consider that V10 changes due to climate change may have a significant impact on offshore wind energy production because the wind power generated depends on the wind speed cubed. Therefore, while offshore wind energy is an agent to fight climate change, it is simultaneously very sensitive to climate change.

Numerous studies have focused on analysing possible future changes in V10 using global climate models (GCMs) and how they may influence wind energy production worldwide or in specific regions. These models can be employed to obtain climate simulations and projections, modelling changes in the physical processes of the atmosphere, ocean, land surface, and cryosphere by considering different scenarios of increasing greenhouse gases

* Corresponding author at: Centro de Investigación Mariña, Universidade de Vigo, Environmental Physics Laboratory (EPhysLab), Campus As Lagoas s/n, Ourense, 32004, Spain.
E-mail address: jose.carlos.fernandez.alvarez@uvigo.es (J.C. Fernández-Alvarez).

https://doi.org/10.1016/j.egyr.2022.12.036

(Stocker et al., 2013). Recently, an extensive selection of GCMs and Earth system models (ESMs) was made available through the 6th phase of the Coupled Model Intercomparison Project (CMIP6) (Eyring et al., 2016). The Scenario Model Intercomparison Project (ScenarioMIP), in particular (O'Neill et al., 2016), occupies a prominent position among the activities covered in this phase, and provides climate projections based on new alternative scenarios of future greenhouse gas emissions and land use (O'Neil et al. 2017) for CMIP6. These updated scenarios are produced with integrated assessment models and driven by the updated pathways of societal development, namely the shared socioeconomic pathways (SSPs) (Riahi et al., 2017). The CMIP6 project and new SSPs were the basis for establishing future climate projections in the most recent IPCC report (IPCC, 2021). Therefore, the GCMs involved in CMIP6 represent the most recent tools for analysing future projections in the context of current climate change.

However, the coarse resolution of GCMs is generally insufficient to provide useful climate change information and impacts for a specific area, particularly where climate and weather are inhomogeneous. This includes areas with complex terrains and tropical regions, where precipitation is strongly driven by convection at finer scales than can be adequately resolved by GCMs. Accurate numerical systems for climate simulation and projection at sufficiently high resolutions are required for effective climate change mitigation and adaptation. The only tool to obtain these high spatial resolution climate projections is regional climate models (RCMs), which can be used to force state-of-the-art CMIP6 GCMs. This process is called dynamic downscaling, and allows for improved understanding of the possible modifications of V10 and the subsequent changes in wind energy resources.

The objective of this work is to project and analyse future changes in V10 and its geographical distribution over the North Atlantic Ocean by means of dynamic downscaling of the CMIP6 project data using the WRF-ARW model. To the best of our knowledge, the present study is the first attempt to analyse the impact of climate change on offshore wind energy and V10 patterns by means of dynamic downscaling in the North Atlantic Ocean (NATL) using CMIP6 data, which contains the most recent future climate projections.

Area under scope

This study focused on analysing V10 changes in the NATL region (Fig. 1a). This region has significant offshore wind energy potential. The North Sea, located in the Atlantic Ocean, has the highest density of offshore wind energy farms worldwide; as a result, North Sea wind energy resources have been studied extensively. Countries such as the United Kingdom, Germany, and China, are global leaders in installed offshore wind energy capacity (GWEC, 2021). The number of offshore wind farms installed in other areas of the North Atlantic is expected to increase over the next few decades due to the development of floating platforms that are suitable for the narrow continental shelf in this area. The first floating offshore wind farm was recently installed along the western Atlantic coast of the Iberian Peninsula (Ramírez et al., 2021). For this reason, the Atlantic coast of the Iberian Peninsula was selected for a more in-depth analysis of the impact future variability in offshore wind energy resources (Fig. 1b). The development of offshore renewable energy is also expected to increase over the next few years along the Atlantic coast of the United States (US) (Fig. 1c) (deCastro et al., 2019; Costoya et al., 2020b) as there is currently little development of this offshore technology (Musial et al., 2016). Finally, future changes in offshore wind energy will also be analysed in the Caribbean Sea (CS) because this area involves many islands with isolated electrical systems, where the development of offshore wind energy is of great interest. In addition, it must be noted that some islands in the Caribbean Sea have already implemented onshore wind farms including Cuba, Curaçao, Jamaica, Martinique, and Guadeloupe (Wright, 2001). Below, various investigations of the changes in V10 and WPD in the future climate for each of these three subregions are detailed.

Regarding the Atlantic coast of the Iberian Peninsula (IP), Soares et al. (2017) used the WRF-ARW model, which was forced by the climatic simulations of the Coordinated Regional Climate Downscaling Experiment (CORDEX) project (scenarios RCP4.5 and RCP8.5), to project future changes in offshore wind power. These authors demonstrated that the majority of climate models project reductions in wind speed and power for all seasons, except for the summer. Moreover, Santos et al. (2018) analysed the variations in the WPD using various RCMs from the CORDEX project, and found a slight increase for the period 2019–2045 under the RCP8.5 scenario. Finally, Costoya et al. (2020a) applied a combination of two bias correction methods to reduce WPD error in climate models and used CORDEX simulations to determine the future WPD reduction across most of the western IP. In addition, they found that a WPD increase was projected for summer months and a decrease in WPD was projected during autumn and spring.

Different authors have investigated future changes in WPD along the Atlantic coast of the US. For example, Liu et al. (2014) used dynamic downscaling to obtain future climate projections from a GCM of the CMIP3 project with the WRF model. They determined that the mean annual wind speed increased from 0.1 to 0.2 m/s in the northern Great Lakes region until the middle of the century. However, until 2090 an even greater increase in the wind speed of 0.1 to 0.4 m/s is projected for this region. In addition, Johnson and Erhardt (2016) determined that the offshore wind resource projections have a slight tendency to decrease along the east coast and increase along the west coast of the US, considering that these changes are less than 2%. These authors used the output from four RCMs from North American Regional Climate Change Assessment Program (NARCCAP), assuming the SRES A2 emission scenario. Recently, Costoya et al. (2020b) used 12 CORDEX simulations of approximately 0.22° spatial resolution to analyse future WPD variations on both the east and west coasts of the US. Overall, the authors found a decline in offshore wind power resource throughout the 21st century in the US, particularly on the east coast.

For the CS subregion, very few studies have focused on the future changes in V10 and WPD. Angeles et al. (2010) found that an increase in easterly winds is expected for this region between 2070 and 2098, especially along the coast. Furthermore, Yao et al. (2016) analysed the differences in wind speed using statistical downscaling of a single GCM (GFDL CM2.1). Finally, Costoya et al. (2019) showed that a maximum annual wind increase of approximately 0.4 m/s is projected for most of the Caribbean at the end of the 21st century, except in the Yucatan Basin. This increase occurred mainly during the rainy season, $\sim$0.5 ms^{-1}. Furthermore, these authors found that a moderate increase in wind, approximately 0.2 m/s is expected during the dry season restricted to the southeast coast. This study was conducted using the CORDEX project at a resolution of approximately 0.44°.

2. Data and methodology

2.1. Data

The outputs of the CESM2 climate model (Community Earth System Model Version 2) (Danabasoglu et al., 2020) from the CMIP6 project were used to run the WRF regional dynamic model with ARW (Advanced Research WRF) dynamic core. These variables were downloaded from the Earth System Grid Federation (ESGF2). These were obtained for the native grid "gn" and with a spatial resolution of 0.9 $\times$ 1.25 ($\sim$1°). In addition, these variables corresponded to a mesh with 288 $\times$ 192 longitude/latitude

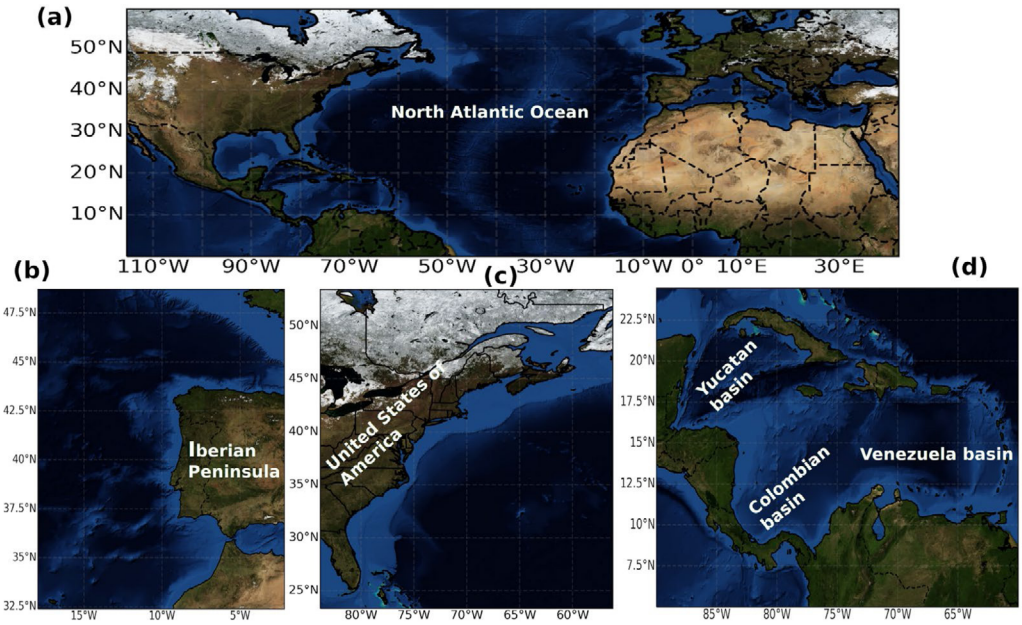

Fig. 1. The area selected for the study of the wind speed of 10 m above sea surface (V10) using the WRF-ARW for the NATL is shown in (a). The subregions for the study on wind power density (WPD) are shown as follows: (b) US East Coast, and (c) Iberian Peninsula, and (d) Caribbean Sea.

and 32 levels. Historical data from 2010–2014 and the scenarios for the three climate projections (MIP Scenario 21C: SSP2-4.5, SSP3-7.0, and SSP5-8.5) were used. These projections cover the intervals 2049–2053 (mid-century (MC)) and 2096–2100 (end-century (EC)). The selection criteria of 5 years are based on achieving stability between the simulation time and the available and necessary computational resources for the runs when using a forced regional model with outputs of a climate model. It is important to mention that several previous analyses have considered time periods in the 5–11 year interval to analyse the impact of climate change on renewable resources, but always considering one scenario or two at most, unlike this research which considers three of the new SSPs (e.g. Alsarraf and Van Den Broeke, 2015; Fant et al., 2016; González et al., 2017; Cai and Breon, 2021; Martinez and Iglesias, 2021).

The CESM2 model selection was based on two main reasons. Firstly, CESM2 has been evaluated for the representation of jet streams and storm tracks, stationary waves, global divergent circulation, annular modes, North Atlantic oscillation, and blocking. Moreover, it ranks within the top 10% of CMIP class models in many of these features (Simpson et al., 2020). In addition, Shen et al. (2022) demonstrated that the CESM2 has the best ability in reproducing the observed near-surface wind speed trends simulated by CMIP6 models. Secondly, CESM2 provides all the necessary variables (see NCAR Technical Notes NCAR/TN 515+STR, Bruyère et al., 2015) to force the WRF-ARW with better resolution compared to the rest of the models that have a resolution of ∼250 km. For its use, it was necessary to process these variables of the different periods to generate the CESM2 intermediate files (26 vertical levels) that were used as the initial and boundary conditions for forcing the WRF-ARW. For it, software was developed in NCL and Fortran based on the methodology proposed by Bruyère et al. (2015) for we can execute el WRF.

The SSPs used in the research present differences; for example, SSP2-4.5 is a scenario that represents the medium part of the range of future forcing pathways and updates the RCP4.5 pathway with a radiative forcing of 4.5 W/m^2 for 2100 (O'Neill et al., 2016). Additionally, SSP2-4.5 features land use and aerosol pathways that are not extreme relative to the other SSPs. In this regard, it is considered that while environmental systems experience degradation, there are some improvements, and overall, the intensity of resource and energy use declines (Riahi et al., 2017). In contrast, the SSP3-7.0 scenario represents the medium to high end of the range of future forcing pathways with radiative forcing of 7.0 W/m^2 in 2100. In particular, SSP3-7.0 is a scenario with both substantial land use changes (particularly decreased global forest cover) and high Near-Term Climate Forcers (NTCF) emissions (particularly SO_2) (O'Neill et al., 2016). Finally, the SSP5-8.5 scenario represents the high end of the range of future pathways. It is the only SSP scenario with sufficiently high emissions to produce a radiative forcing of 8.5 W/m^2 in 2100, according to O'Neill et al. (2016).

The V10 simulated using WRF-ARW was evaluated with respect to the ERA5 reanalysis (Hersbach et al., 2020). ERA5 is the most recent (5th generation) global atmospheric reanalysis of the European Centre for Medium-Range Weather Forecasts (ECMWF) and stands out for its high resolution (31 km horizontally and 137 vertical levels) as well as for a large amount of assimilated historical observations. This represents a significant improvement over its predecessor, ERA-I reanalysis. The characteristics of the surface and low-level winds in ERA5 over the ocean, in relation to observations and other reanalyses, have been evaluated by numerous investigations (e.g., Olauson, 2018; Belmonte and Stoffelen, 2019; Kalverla et al., 2019) and ERA5 has been found to work well for the representation of these fields.

2.2. Model setup and methodology

As mentioned in the Introduction, the objective of this work is mainly to analyse the future changes for V10 in future climate (mid- and end- of the century) and their implications in the offshore WPD for selected regions of interest (IP, US and CS). The flowchart of the research is explained below: (1) simulations with dynamic downscalling are performed using WRF-ARW forced by historical CESM2 data, (2) an evaluation of the configuration is then carried out with respect to ERA5 reanalysis data. Once the configuration has been evaluated, (3) the future conditions are simulated to study future changes of the V10 field in the Atlantic Ocean and (4) the WPD variable is then regionalized for IP, US

and CS and the future projections are analysed. A more detailed explanation is presented below.

Dynamic downscaling was performed with WRFv3.8.1 (Skamarock et al., 2008) using the ARW dynamic core. This was forced using the CESM2 model outputs every 6 h. The simulations have 40 vertical layers from the surface to 50 hPa and 480 × 800 grids with a horizontal spacing of 20 km centred on the North Atlantic Ocean. The parameterizations employed in the WRF-ARW setup are as follows: the WSM6 microphysics scheme (Hong and Lim, 2006), Yonsei University PBL scheme (Hong et al., 2006), revised MM5 surface layer scheme (Jimenez et al., 2012), United Noah Land Surface Model (Tewari et al., 2004), shortwave and longwave RRTMG schemes (Iacono et al., 2008), and Kain–Fritsch ensemble cluster scheme (Kain, 2004). These have been used in several investigations in the region within the computational domain of WRF-ARW by Insua-Castro and Miguez-Macho (2018) and Insua-Castro et al. (2019). On the other hand, spectral nudging of waves longer than 1000 km is employed to avoid distortion of the large-scale circulation within the regional model domain owing to the interaction between the model solution and lateral boundary conditions (Miguez-Macho et al., 2004). For the WRF-ARW simulations, a 6-month spin-up was performed before the period to be simulated, and the restart mode was used when the WRF-ARW was stopped.

The WPD was calculated by considering the V10 field of the WRF-ARW outputs. WPD (W/m^2) represents the energy available at a specific site that can be converted by a wind turbine. This value was calculated using the following equation:

$$WPD = \frac{1}{2}\rho v^3 \tag{1}$$

where ρ represents the density of air with a value of approximately 1225 kg/m^3 at sea level and at 15 °C (Salvador et al., 2018; Ulazia et al., 2019), and v is the wind speed (m/s). To determine the WPD, the wind speed data were extrapolated up to 120 m, which is the typical height of marine wind turbines (Swart et al., 2009) considering an atmosphere with neutral stability. The wind speed values were extrapolated following the expression of the logarithmic wind profile:

$$u_z = u_{zm} * ln\left(\frac{h}{z_0}\right) / ln\left(\frac{h_m}{z_0}\right) \tag{2}$$

where u_{zm} is the wind speed near the surface (m/s), h_m is the height (m) at which the wind is measured near the surface (10 m in this study), u_z is the mean wind speed (m/s) at the extrapolated height (h) of 120 m, and z_0 is the local roughness length (a value of 1.52×10^{-4} m above the ocean surface is considered). This method has been used by Yamada and Mellor (1975) and Salvador et al. (2018) in previous research. The WPD was calculated for the WRF-ARW domain, but was analysed mainly in the IP, US, and CS subregions. This methodology is considered and not a mathematical interpolation to obtain the wind at 120 m to be able to compare the results as homogeneous as possible with previous investigations where this physical relationship has been considered.

Subsequently, to use this configuration of WRF-ARW to simulate future projections with different SSPs, it was evaluated in comparison with ERA5. This analysis was performed on the area shown in Fig. 1a. The statistical graphs presented in Table 1 were used, where x_i and y_i are the simulated and observed values, respectively, and n is the number of data points. In addition, $\overline{x_i}$ and $\overline{y_i}$ are the mean values of the simulations and observations, respectively. Furthermore, the evaluation and analysis of the different SSPs were conducted annually and seasonally. In this case, boreal winter (JFM), spring (AMJ), summer (JAS), and autumn (OND) are considered for the analysis of the IP and US subregions. However, for the CS the dry season (DS) from December to April and wet season (WS) from May to November are considered because the Caribbean climate is characterized by two seasons (Enfield and Alfaro, 1999). From here on, the simulations with the historical CESM2 for 2010–2014 will be referred to as WRF-CESM2_HIST, and for the climatic scenarios, it will be WRF_CESM2_x_MC or WRF_CESM2_x_EC, where *x* represents the SSPs and MC or EC the time periods. Fig. 1b–d shows the areas considered in the WPD study.

Table 1
Statigraphs used in the evaluation of the configuration of the WRF-ARW.
Source: Modified from Brown et al. (2013).

Statigraphs	Equation
Absolute error (MAE)	$\frac{\sum_{i=1}^{n} \lvert x_i - y_i \rvert}{n}$
Root mean square error (RMSE)	$\sqrt{\frac{\sum_{i=1}^{n} (x_i - y_i)^2}{n}}$
Pearson's correlation (R)	$\frac{\sum_{i=1}^{n} (x_i - \overline{x_i})(y_i - \overline{y_i})}{\sqrt{\sum_{i=1}^{n} (x_i - \overline{x_i})^2 (y_i - \overline{y_i})^2}}$
Bias (B)	$\frac{\sum_{i=1}^{n} (x_i - y_i)}{n}$

3. Results and discussion

3.1. Evaluation of the downscaling methodology

Fig. 2 shows the V10 field for WRF-ARW_HIST and ERA5 for the period 2010–2014. In addition, the spatial differences calculated from WRF-ARW_HIST and ERA5 were presented. Overall, spatial differences were less than 1 m/s in the North Atlantic region. In winter, WRF-CESM2_HIST shows a greater wind speed than ERA5 in the region between 40–50°N that extends mainly towards the coast of Europe. However, the opposite was observed in the tropical and subtropical latitudes, where speeds lower than ERA5 were detected. For spring and summer, similar behaviour was observed with two zones where wind speed was overestimated, one near the coast of the US and another from the central Atlantic to the coast of Western Europe. For autumn, the WRF-CESM2_HIST projections showed a tendency to underestimate the wind speed (<1 m/s) in most of the North Atlantic. Annually, simulated data show very similar behaviour with spatial differences of ∼0.8 m/s or less across the entire study region. It should be highlighted that WRF-ARW_HIST shows an adequate representation compared to ERA5 in areas where future changes in the WPD will be studied.

A summary of the previously proposed statistics is shown in Fig. 3. The Pearson correlation coefficients present values higher than 0.8 in all the time periods studied and are lower during summer. The MAE varies from 0.5 to 1 m/s, being higher in summer and lower in autumn, with an annual value of ∼0.5 m/s. On the other hand, B increases from winter to summer and decreases considerably for autumn, presenting a mean value for the entire period of ∼0.1 m/s; which is an overestimation. Finally, the RMSE presents values that oscillate between 0.8 and 1.2 m/s and are ∼0.6 m/s annually. In general, the use of the forced WRF-ARW model with the CESM2 provides an adequate representation of V10.

3.2. Future changes for V10 North Atlantic Ocean determined using WRF-ARW and SSPs

Future changes will be determined as the difference between the simulations using the WRF-ARW forced with different SSPs minus the WRF-ARW forced with historical data from the CMIP6.

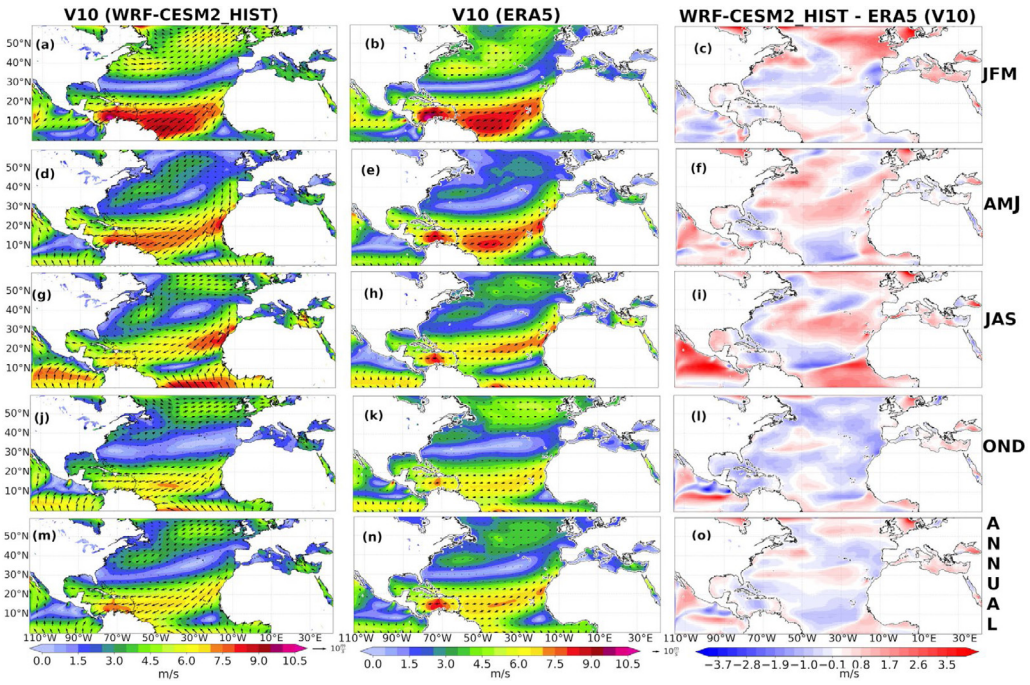

Fig. 2. The V10 fields for WRF-CESM2_HIST (first column) and ERA5 (second column) and the spatial difference (third column). The fields displayed from top to bottom correspond to boreal winter (JFM), spring (AMJ), summer (JAS), autumn (OND), and annually (ANNUAL) values. The modular value of V10 is represented by contours and the direction of V10 by arrows. Historical period: 2010–2014.

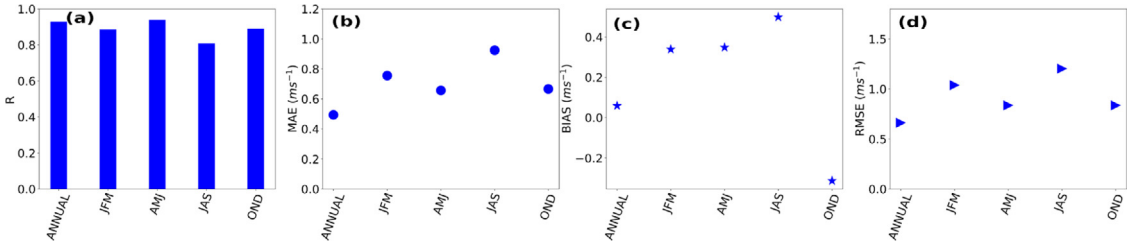

Fig. 3. Statigraphs calculated with the WRF-CESM2_HIST simulations and the ERA5 reanalysis of the V10 field for the study area (Fig. 1a). (a) R, (b) MAE, (C) B and (d) RMSE. Historical period: 2010–2014.

Therefore, positive values indicate future increases and negative values indicate decreases. Future changes were determined for the mid-21st century (2049–2053) and the end of the 21st century (2096–2100). Fig. 4 shows the comparison of V10 from WRF-ARW_HIST and the differences in the simulations of WRF-ARW for each SSP with respect to the MC. Considering SSP2-4.5, a decrease was expected above latitudes of 30°N during winter for the MC period (Fig. 4b). However, positive values prevailed south of 30°N, with the exception of the eastern Caribbean Sea. In spring, a decrease was maintained across most of the North Atlantic Ocean, except in the Caribbean Sea. Positive values prevailed for summer and autumn, with the exception of the southern region of the US coast (Fig. 4j, n). An increase was projected in most tropical regions, with little annual change in the rest of the study area (Fig. 4r).

On the other hand, using SSP3-7.0 for winter, the tendency for V10 to decrease continues to be represented, with two exceptions: the Iberian Peninsula and the West African zone (see Fig. 4c). In spring, negative values increased throughout the area, and were greater than those observed using SSP2-4.5. Moreover, mainly positive values for summer and autumn are expected over the CS, the US coast, and IP, but the values were relatively lower than those shown for SSP2-4.5 (Fig. 4j, n). Regarding the annual average, there is a tendency to show little change, with the exception of the tropical zone near the coast of Africa and northwest of the Iberian Peninsula (Fig. 4s). Considering SSP5-8.5, the most significant changes occur in winter, with a considerable decrease (∼3.5 m/s) in the Caribbean Sea, along the African coast, and latitudes above 50°N (Fig. 4d). A few changes in the general form can be seen for EC compared to MC considering SSP2-4.5 and SSP3-7.0. However, under SSP5-8.5, positive values were expected throughout the North Atlantic Ocean region for summer and autumn, showing an increasing trend with more extreme conditions at the end of the 21st century (Figure S1).

In general, these results differ from previous research (e.g., Collins et al., 2013; Gallagher et al., 2016) which found that the average wind changes due to climate change over the North Atlantic Ocean at the end of the 21st century were small and negative. These authors used data corresponding to CMIP5 models to obtain the results. However, this research showed a notable increase for summer and autumn, mainly in the tropical zone and areas near the coast of Western Europe. This result is similar to that reported by Ruosteenoja et al. (2019), wherein the frequency of strong westerly geostrophic winds was found to increase by 50% in northern Europe and the northern North Atlantic Ocean in autumn. In addition, the projected increase in the tropical region is in correspondence with the projected increase for WPD over most mid- to low-latitudes ocean areas (30°S–30°N) according to Zheng et al. (2019). Finally, these projections are in correspondence with that found for the surface wind speed for the period

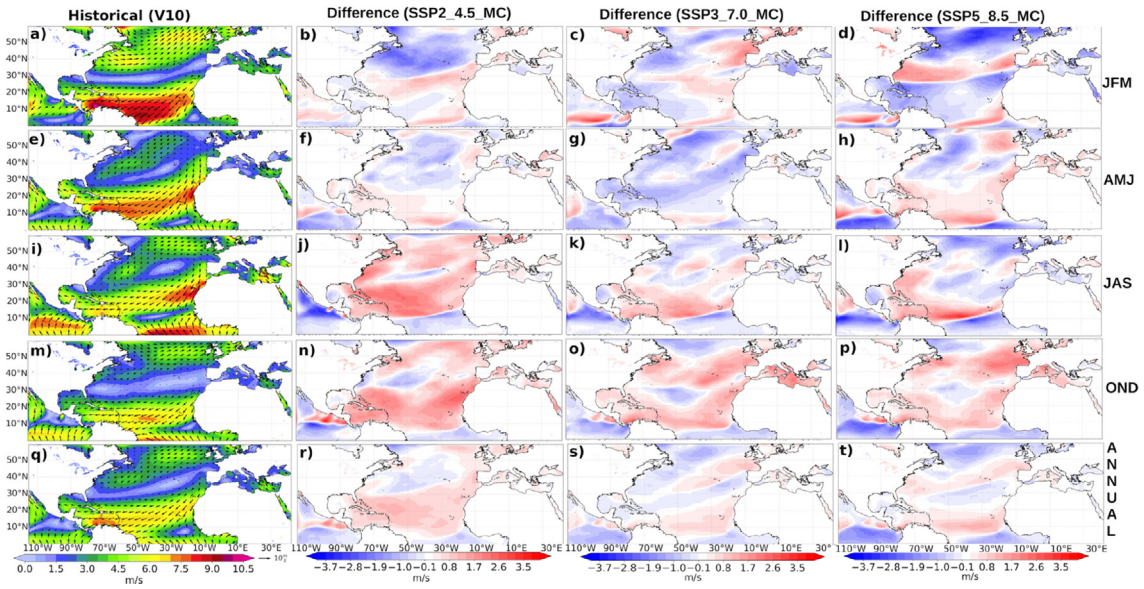

Fig. 4. The V10 for the historical period and the differences in the simulations of WRF-ARW for each SSP. The fields displayed from top to bottom correspond to boreal winter (JFM), spring (AMJ), summer (JAS), autumn (OND), and annually (ANNUAL), respectively. The modular value of V10 is represented by the contours and direction of V10 by the arrows. Period: 2049–2053 (MC).

1988–2011 by Zheng et al. (2016). These authors show positive trends (5–11 (cm/s)/yr) in the North Atlantic region mainly on the east coast of the United States, northwest Africa, and the Atlantic coast of the IP extending to the Cantabrian Sea using Cross-Calibrated, Multi-Platform (CCMP) wind data.

3.3. Future changes for WPD in the Iberian Peninsula subregion

Fig. 5 shows a comparison of the historical WPD and differences in the WRF-ARW simulation results for each SSP with respect to the WPD for the Iberian Peninsula. Under SSP2-4.5, the WPD is projected to decrease in winter, with maximum values occurring in the north of the IP. In spring, positive values for WPD were projected for most of the west coast of the IP, but considerable increases were noted in the northwestern corner of the IP (Fig. 5f). Positive values were observed very close to the coast of the Iberian Peninsula in summer (>100 W/m^2), but the coast of Galicia to the north of Portugal stood out. Furthermore, few changes were expected in autumn and annually (Fig. 5n, r). Considering SSP3-7.0, an increase is projected for winter, with a maximum in the north of Galicia; however, a notable decrease in the entire coast of the IP is expected for spring (Fig. 5c, g). This behaviour is contrary to the previous scenario analysed for both seasons. On the other hand, increases are projected northwest of the IP for summer and autumn, but there is very little change in the annual analysis (Fig. 5k, o). Considering SSP5-8.5, the most notable difference is the increase projected for the north of the IP for the autumn.

Regarding the EC period and considering all SSPs (see Fig. 6), positive changes were projected to the north of the IP in winter, extending up to 40°N. The intensity of the changes was greatest for SSP5-8.5. A similar pattern was noted in summer, where positive differences with greater magnitudes are expected for the WPD considering the projected scenario in which emissions are high enough to create a radiative forcing of 8.5 W/m^2 in 2100 (see Fig. 6). This result could be related to the increase in V10 at the end of the 21st century in this region, as described in the previous section.

In summary, according to the SSPs, a considerable increase is expected for autumn and summer for both study periods, although slight annual WPD variations were detected, especially in summer. Previous studies (e.g.,; Soares et al., 2017; Moemken et al., 2018; Costoya et al., 2020a; Carvalho et al., 2021) have shown a projected increase for this subregion but always with a slight discrepancy in percentage values. Therefore, summer is maintained as the season with the greatest increase, which will allow a higher stability of the offshore energy resource throughout the year, as this is the season with the lowest WPD on average. Stable wind power generation benefits the gathering and conversion of wind energy, whereas unstable WPD negatively affects the productivity of wind energy conversion (Zheng and Pan, 2014; Zheng, 2018). Moreover, for MC, different behaviours are expected for winter, where SSP2-4.5 and SSP5-8.5 project a decrease, and SSP3-7.0 does not. This may be attributed to the fact that SSP3-7.0 is a scenario involving substantial land use change (particularly decreased global forest cover) and high NTCF emissions (particularly SO_2). However, for EC, a notable increase is expected for all the SSPs north of the Iberian Peninsula. These results coincide with those of Costoya et al. (2020a), which projected an increase for this period but used the RCP8.5 scenario. Also, Zheng et al. (2019) project for the period 2080–2099 an increase of 100–150 W/m^2 for the west coast of the IP with a maximum in the north-northwest. Finally, using ERA-Interim data (1979–2014), Zheng et al. (2022) show a significant (at 95% level) positive annual trend for WPD (1–2 (W/m^2)/yr) in the Atlantic coast of the IP. This shows that there is correspondence between the results of this research and what was found for past climate.

3.4. Future changes for WPD in the US subregion

According to SSP2-4.5, the WPD in winter is projected to decrease at latitudes above 35°N with maximum values along the Maine, Massachusetts, New Hampshire, and New Jersey coasts, for the period 2049–2053 (Fig. 7b). During summer positive WPD values were projected mainly along the North Carolina, South Carolina, and Virginia coasts (Fig. 7j). Negligible changes were observed during the other periods. Additionally, when considering SSP3-7.0, the WPD was projected to decrease in winter (Fig. 7c). However, a different behaviour in autumn is expected along with an increase in the northernmost states of the US (Fig. 7o). The remaining periods exhibited a few distinct and significant changes.

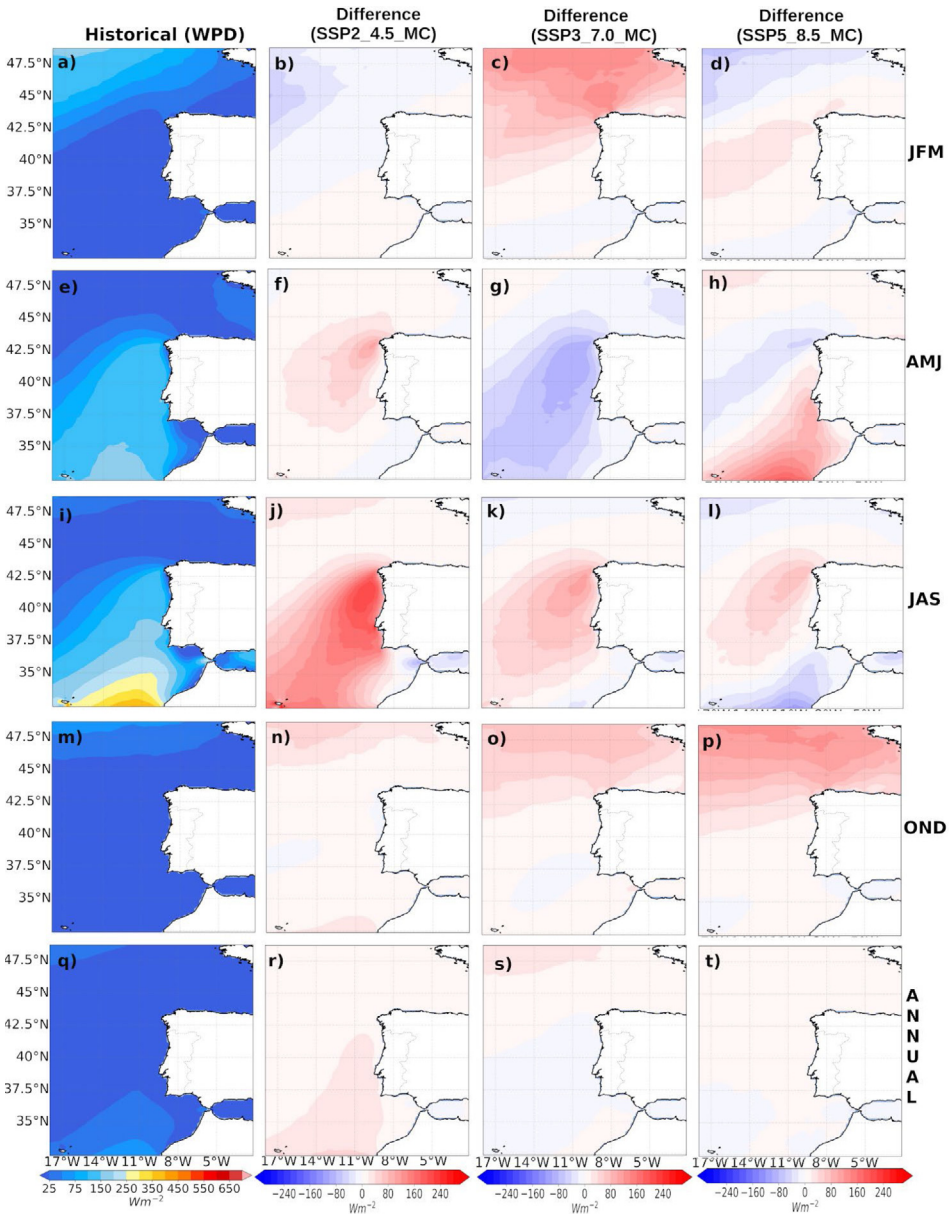

Fig. 5. The WPD for the historical period and the differences between the simulations of WRF-ARW for each of the SSPs in the IP subregion. The boreal winter (JFM), spring (AMJ), summer (JAS), autumn (OND), and annually (ANNUAL) fields are displayed from top to bottom. Period: 2049–2053 (MC).

Fig. 7d shows the behaviour using SSP5-8.5, where there is a different pattern, with positive values below 40°N and negative values above 40°N. In general, the rest of the periods show little change, except in summer, where there is some correspondence with SSP2-4.5 and the positive values are projected for states near 35°N. During 2096–2100, the most significant changes are the maximum decreases in WPD values according to SSP3-7.0 and the increase in summer as per SSP5-8.5 (Fig. 8).

In general, there is a decrease in WPD in winter considering all SSPs, an increase in summer, and little change over the remaining periods, except in autumn, as it is expected that towards the end of the 21st century, a slight increase in WPD will occur in the northern region of the Atlantic coast. These results correspond with those of Costoya et al. (2020b) but differ from those of Kulkarni and Huang (2014), who determined a decrease in WPD during summer and an increase during winter. This study corroborated the findings of Costoya et al. (2020b), which showed that the central zone of the east coast of the US (e.g., Virginia, North Carolina, and South Carolina) constitutes an important target area for the present as well as the future, as it presents good conditions for wind resource development. It was also observed that the northern section, mainly the coastline of the states of Maine, Massachusetts, and New Hampshire, also has a projected increase in WPD. Besides, Zheng et al. (2022) show that the US Atlantic coast has a significant positive annual trend at 95% level for WPD (2–4 (W/m^2)/yr) but based on the ERA-Interim wind product.

3.5. Future changes for WPD in the Caribbean Sea subregion

In the analysis of the Caribbean Sea subregion, it must be considered that only two seasons are considered (dry (DS) and wet (WS)); hence, analyses will be carried out for these seasons and for the annual variation. Considering SSP2-4.5 for 2049–2053 in the DS, a strengthening of the WPD pattern is projected compared to the historical pattern for the Venezuelan Basin that extends to the Caribbean Sea. However, there was a slight decrease in WPD values close to the coast of Colombia (Fig. 9b). Regarding the WS, a more notable increase is projected with respect to the

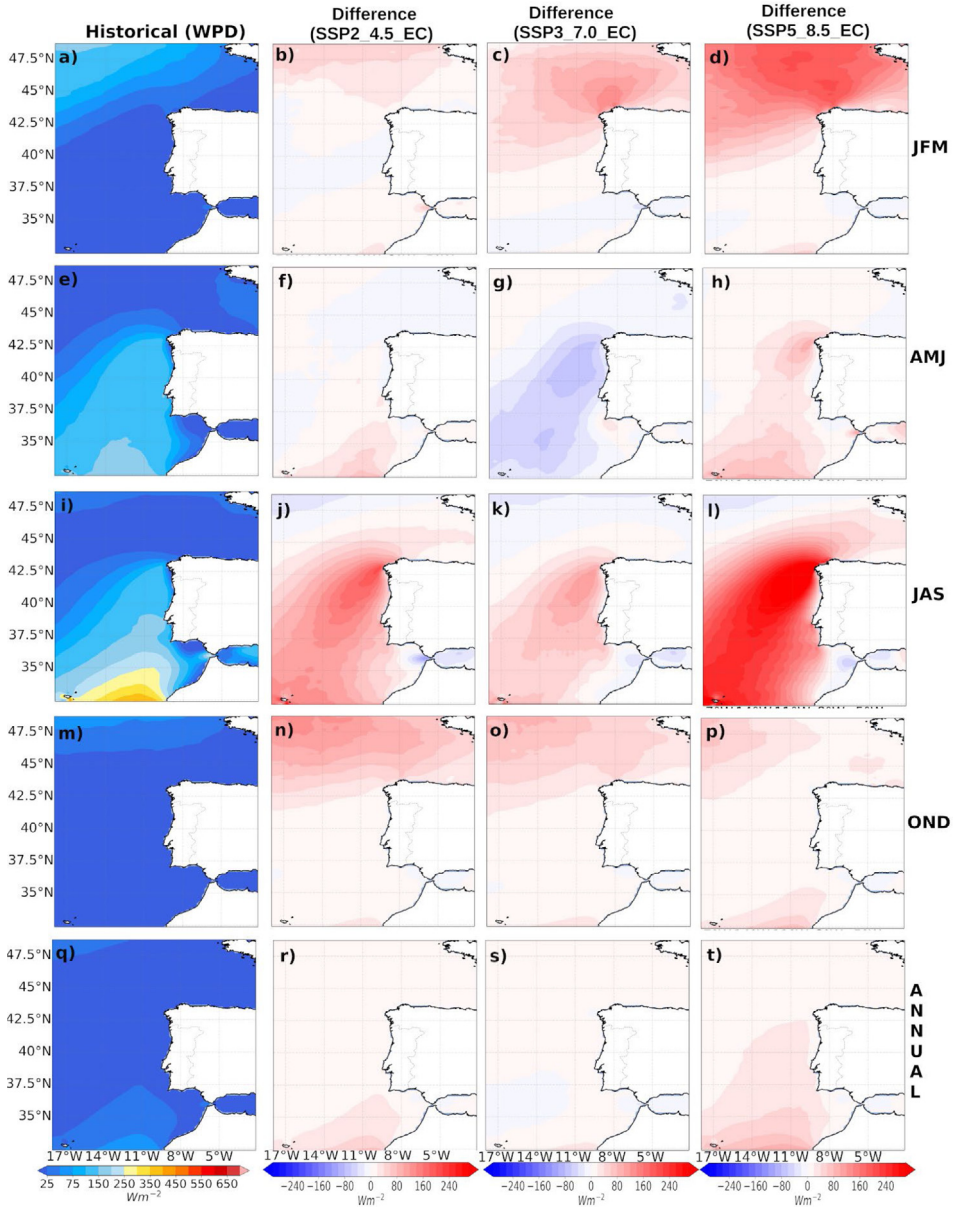

Fig. 6. The WPD for the historical period and the differences between the simulations of WRF-ARW for each of the SSPs in the IP subregion. The boreal winter (JFM), spring (AMJ), summer (JAS), autumn (OND), and annually (ANNUAL) fields are displayed from top to bottom. Period: 2096–2100 (EC).

historical WPD (see Fig. 9f), with maximum values located in the Colombian Basin, Venezuela Basin, near the south and north coast of Española, and in the eastern region of Cuba. However, little change is expected in the Yucatan Basin. As an annual average, an increase is projected mainly over the Venezuelan Basin with values of 80–160 W/m^2 (Fig. 9j).

Considering SSP3-7.0, it is projected that there will be a decrease over the entire CS area during the DS, with maximum values occurring in the Colombian Basin. However, the behaviour will be different in the WS, where an increase is expected near the coast of Colombia and Venezuela, but limited significant changes projected for the rest of the study area (see Fig. 9c, g). The annual average changes will be insignificant, except for along the coast of Colombia (mainly along the Barranquilla and San Marta coastal states). The expected changes for MC considering SSP5-8.5 are similar to the patterns obtained using SSP3-7.0, but differ from those observed considering SSP2-4.5, which projects a majority increase throughout the entire region.

For the period 2096–2100, a decrease in the WPD values in the Yucatan and Colombia basins was projected for all SSPs in the DS, but a slight increase was observed in the Venezuela Basin (Fig. 10b, c, d). For the rest of the periods analysed, a notable increase in WPD values (>240 W/m^2) was projected throughout the CS, with the exception of the Yucatan Basin, which showed little change (Fig. 10). The results are similar to those obtained by Costoya et al. (2019) using the RCP8.5 and CORDEX scenario data. Costoya et al. (2019) found a decrease in wind energy for most of the Caribbean region during the dry season at the end of the 21st century, with the Colombian Basin standing out and a moderate increase in wind energy in the Venezuela Basin. In contrast, during the WS, they detected an increase in wind energy in the Colombian and Venezuelan basins with a decrease in the wind energy for the Yucatan Basin with maximum values projected at the middle of the 21st century, but little change towards the end of the 21st century. In general, the most notable projected increase in the WPD is expected in the wet season over the Colombian basin, being higher under the SSP585 scenario at

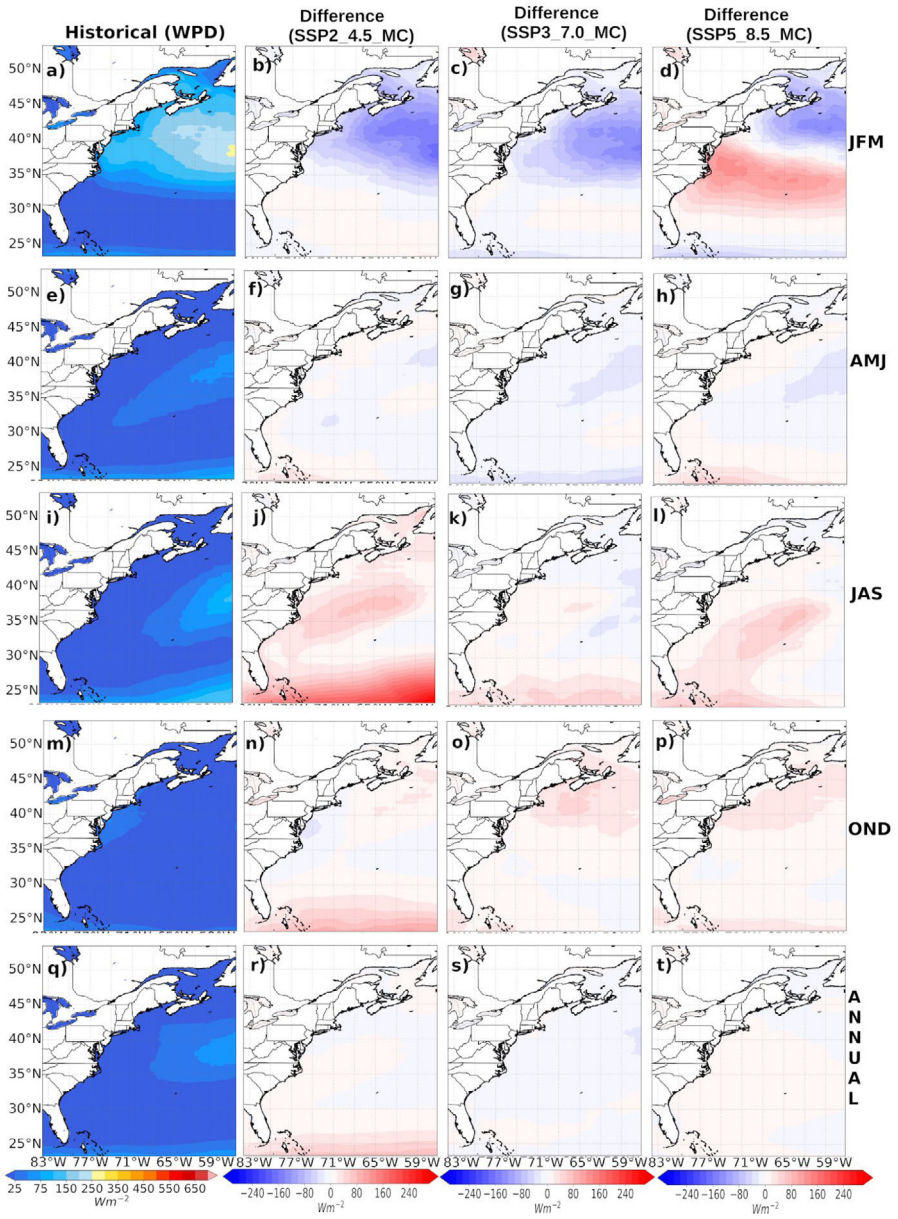

Fig. 7. The WPD for the historical period and the differences between the simulations of WRF-ARW for each of the SSPs in the US subregion. The boreal winter (JFM), spring (AMJ), summer (JAS), autumn (OND), and annually (ANNUAL) fields are displayed from top to bottom. Period: 2049–2053 (MC).

the end of the century. This may be associated with the increase in wind speed in this area (Fig. 4, S1). This variable, in turn, could be related to the expected increase in sea surface temperature throughout the basin and to the decrease in sea level atmospheric pressure towards the southern Caribbean Sea, reported by Bustos-Usta and Torres-Parra (2021). The former would affect wind shear and thus increase wind speed (Vecchi and Soden, 2007; Nolan and Rappin, 2008), while the latter would increase spatial gradients of atmospheric pressure. An increase in wind speed was found by Bustos-Usta and Torres-Parra (2022) especially towards the south of the Colombian basin. Finally, Zheng et al. (2019) observed an increase (>150 W/m^2) of WPD in the period 2080–2099 with respect to the historical period mainly in the Colombian basin.

4. Conclusion and remarks

In this study, we investigated large-scale future changes in the V10 patterns for the North Atlantic Ocean and in terms of WPD for the three subregions of interest in the context of climate change. Dynamic downscaling was performed using the WRF-ARW and CESM2 climate scenarios which belong to CMIP6 project. The results of this research provide more information on future changes for the variable V10 and its influence on WPD, but with the advantage of considering high spatial resolution data and several scenarios with different characteristics and having a representation of different radiative forcing of low–medium–high scale in the spectrum according to the IPCC. To the best of our knowledge, this is the first study to carry out dynamical downscaling of CMIP6 data with the aim of analysing offshore wind energy resources in the North Atlantic Ocean.

Overall, the projected future changes in V10 show a decrease for the winter and spring seasons, with some exceptions where positive values are projected such as the west coast of the Iberian Peninsula and Africa. For summer and autumn, the increase was notable for most of the North Atlantic Ocean, but with maximum values seen in the tropical region on an annual scale. In addition, the changes intensify towards the end of the 21st century, and these are greater considering SSP5-8.5. Moreover, for the Iberian

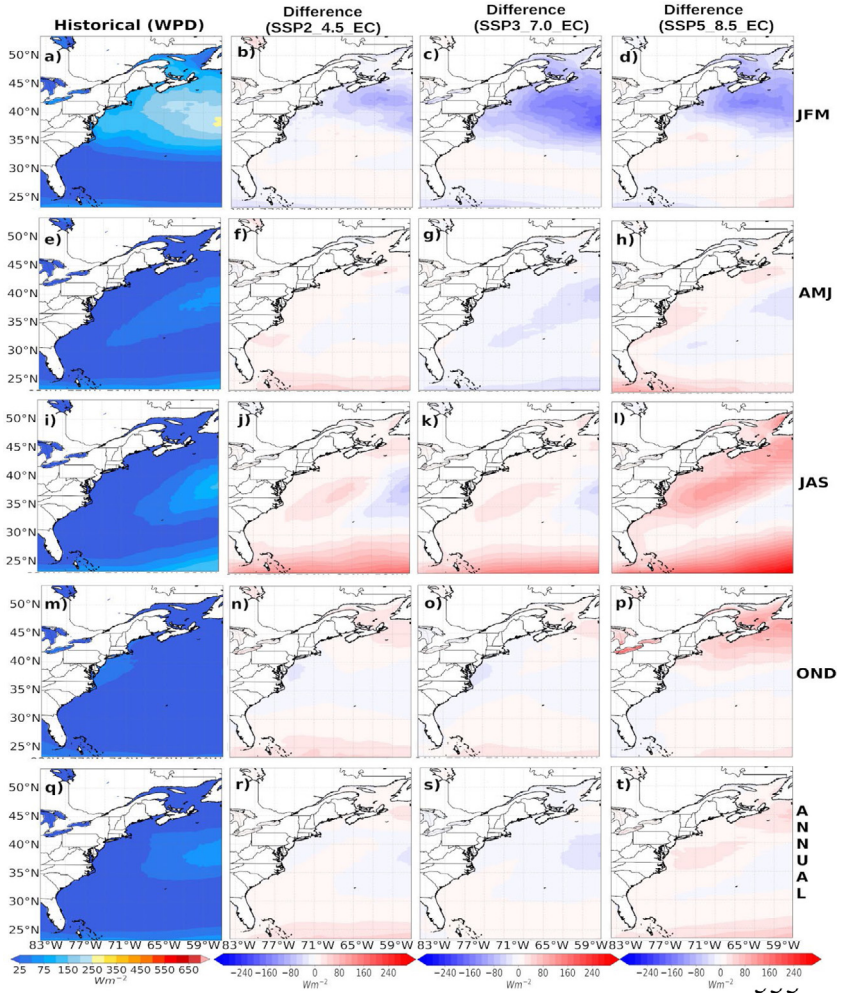

Fig. 8. The WPD for the historical period and the differences between the simulations of WRF-ARW for each of the SSPs in the US subregion. The boreal winter (JFM), spring (AMJ), summer (JAS), autumn (OND), and annually (ANNUAL) fields are displayed from top to bottom. Period: 2096–2100 (EC).

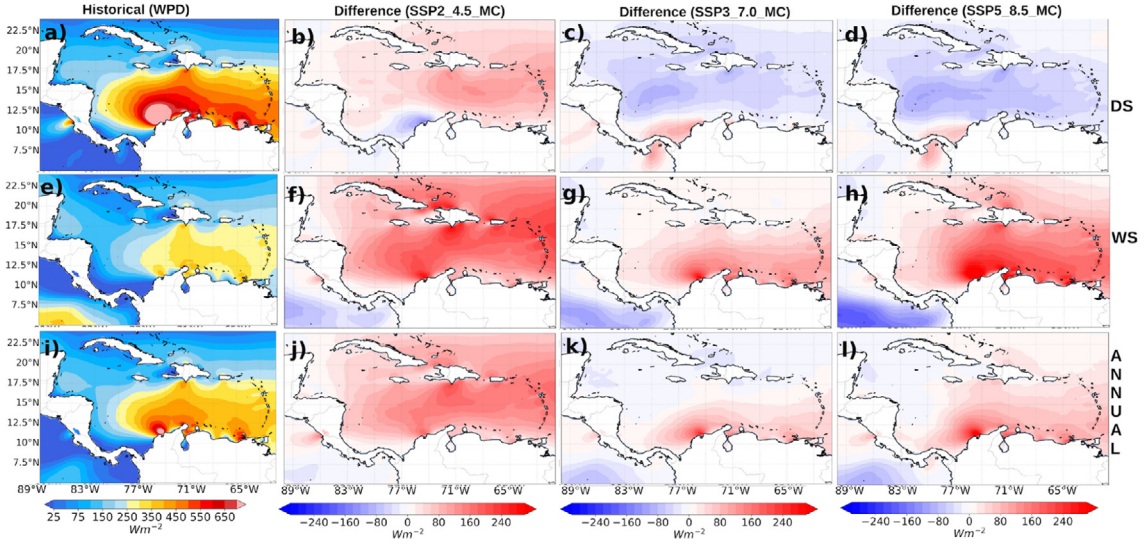

Fig. 9. The WPD for the historical period and the differences between the simulations of WRF-ARW for each of the SSPs in the Caribbean Sea subregion. The dry season (DS), wet season (WS), and annually (ANNUAL) fields are displayed from top to bottom. Period: 2049–2053 (MC).

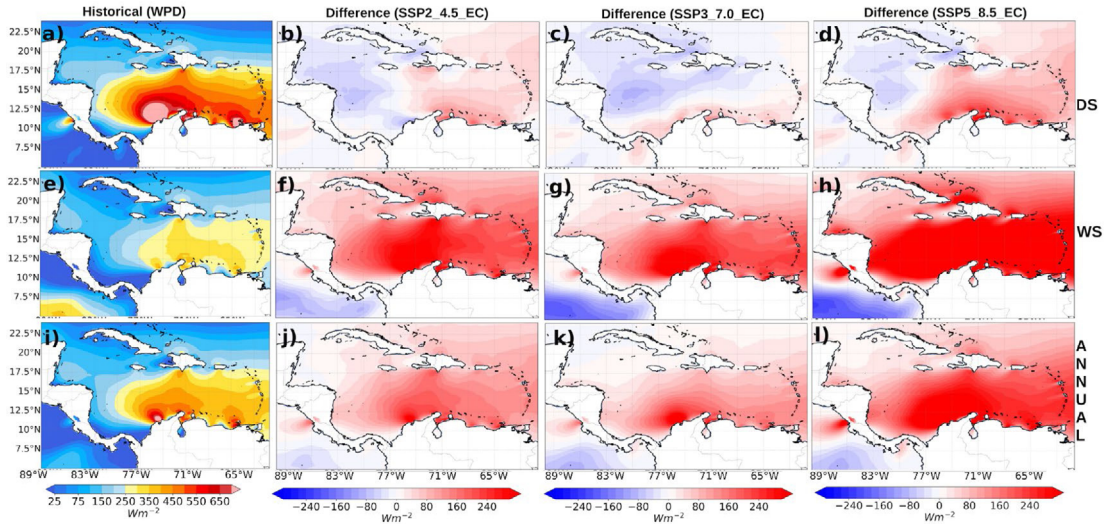

Fig. 10. The WPD for the historical period and the differences between the simulations of WRF-ARW for each of the SSPs in the Caribbean Sea subregion. The dry season (DS), wet season (WS), and annually (ANNUAL) fields are displayed from top to bottom. Period: 2096–2100 (EC).

Peninsula subregion, using the SSPs, will project a considerable increase in autumn and summer for the middle and end of the 21st century. Towards the middle of the 21st century, WRF-ARW using SSP2-4.5 and SSP5-8.5 project a decrease in V10 in winter, except for SSP3-7.0. However, by the end of the 21st century, a notable increase was projected for all the SSPs north of the Iberian Peninsula.

Regarding the US subregion and considering all SSPs, a decrease in WPD is projected in winter and an increase in summer, with limited changes foreseen for the remaining periods. Autumn, for example, is expected to show a slight increase in the northern region of the Atlantic coast at the end of the 21st century. Therefore, the Virginia, North Carolina, and South Carolina coastlines constitute potential wind resource development areas in the future. For the Caribbean Sea subregion, according to the SSPs, a decrease is projected in the dry season in the Yucatan and Colombia basins, which became more pronounced at the end of the 21st century. However, a considerable annual increase in offshore wind power is expected for the Colombia and Venezuela basins and the region north of Española and Cuba. Minimal change was projected for the rest of the area.

The present analysis represents the first attempt to provide WPD projections at high spatial resolution for the whole North Atlantic Ocean. In addition, three areas where a future development of the offshore wind energy industry is expected were analysed more in detail because this information can help policymakers to adapt or modify strategies to improve the efficiency of future offshore wind farms. The approach used in the present analysis can be extended in future research with the aim of downscaling more GCMs to increase the robustness of the results. In addition, the time period and the SSPs can be increased to provide a greater representation of the WPD changes towards the middle and end of the 21st century.

CRediT authorship contribution statement

José C. Fernández-Alvarez: Conceptualization, Methodology, Software, Writing – original draft, Writing – review & editing, Data curation, Formal analysis. **Xurxo Costoya:** Conceptualization, Methodology, Writing – review & editing, Formal analysis. **Albenis Pérez-Alarcón:** Data curation, Software, Methodology, Formal analysis. **Stefan Rahimi:** Software, Data curation. **Raquel Nieto:** Conceptualization, Writing – review & editing, Investigation, Supervision. **Luis Gimeno:** Conceptualization, Writing – review & editing, Investigation, Supervision.

Declaration of competing interest

The authors declare that they have no known competing financial interests or personal relationships that could have appeared to influence the work reported in this paper.

Data availability

ERA5 reanalysis data can be obtained from https://cds.climate.copernicus.eu/cdsapp#!/dataset/reanalysis-era5-single-levels-monthly-means?tab=form and CESM2 model data from https://esgf-data.dkrz.de/search/cmip6-dkrz/. The WRF-ARW outputs are available upon request to the corresponding author.

Acknowledgements

José C. Fernández-Alvarez acknowledge the support from the Xunta de Galicia under the grant no. ED481A-2020/193. Albenis Pérez-Alarcón acknowledges a PhD grant from the University of Vigo. José C. Fernández-Alvarez and Albenis Pérez-Alarcón thank the EU-IACOBUS scholarship. Xurxo Costoya is supported by the Spanish Government through a Juan de la Cierva Postdoctoral Fellowship (JC2020-043745-I). This work is supported by the SETESTRELO project (PID2021-122314OB-I00) funded by the Ministerio de Ciencia, Innovación *y* Universidades, Spain. Partial support was also obtained from the Xunta de Galicia under the project "Programa de Consolidación e Estructuración de Unidades de Investigación Competitivas (Grupos de Referencia Competitiva)" (ED431C 2021/44). In addition, this work has been possible thanks to the computing resources and technical support provided by CESGA (Centro de Supercomputación de Galicia).

Appendix A. Supplementary data

Supplementary material related to this article can be found online at https://doi.org/10.1016/j.egyr.2022.12.036.

References

Alizadeh-Choobari, O., Zawar-Reza, P., Sturman, A., 2014. The wind of 120 days and dust storm activity over the Sistan Basin. Atmos. Res. 143, 328–341. http://dx.doi.org/10.1016/j.atmosres.2014.02.001.

Alsarraf, H., Van Den Broeke, M., 2015. Using the WRF regional climate model to simulate future summertime wind speed changes over the Arabian Peninsula. J. Climatol. Weather Forecast. 1–8. http://dx.doi.org/10.4172/2332-2594.1000144.

Angeles, M.E., González, J.E., Erickson, III.D.J., Hernández, J.L., 2010. The impacts of climate changes on the renewable energy resources in the Caribbean region. J. Sol. Energy Eng. 132, 031009-1-031009-13. http://dx.doi.org/10.1115/1.4001475.

Belmonte, Rivas M., Stoffelen, A., 2019. Characterizing ERA-Interim and ERA5 surface wind biases using ASCAT. Ocean Sci. 15, 831–852. http://dx.doi.org/10.5194/os-15-831-2019.

Brown, B., Ebert, E., Fowler, T., Gilleland, E., Kucera, P., Wilson, L., 2013. Verification Methods for Tropical Cyclone Forecasts. WMO Technical Document WWRP 2013-7, p. 7.

Bruyère, C.L., Monaghan, A.J., Steinhoff, D.F., Yates, D., 2015. Bias-corrected CMIP5 CESM data in WRF/MPAS intermediate file.

Bustos-Usta, D.F., Torres-Parra, R.R., 2021. Ocean and atmosphere changes in the Caribbean Sea during the twenty-first century using CMIP5 models. Ocean Dyn. http://dx.doi.org/10.1007/s10236-021-01462-z.

Bustos-Usta, D.F., Torres-Parra, R.R., 2022. Projected wind changes in the Caribbean Sea based on CMIP6 models. Clim. Dyn. 1–15. http://dx.doi.org/10.1007/s00382-022-06535-3.

Cai, Y., Breon, F.M., 2021. Wind power potential and intermittency issues in the context of climate change. Energy Convers. Manage. 240, 114276. http://dx.doi.org/10.1016/j.enconman.2021.114276.

Carvalho, D., Rocha, A., Costoya, X., deCastro, M., Gómez-Gesteira, M., 2021. Wind energy resource over Europe under CMIP6 future climate projections: What changes from CMIP5 to CMIP6. Renew. Sust. Energ. Rev. 151, 111594. http://dx.doi.org/10.1016/j.rser.2021.111594.

Collins, M., et al., 2013. Long-term climate change: projections, commitments and irreversibility. In: Climate Change 2013-the Physical Science Basis: Contribution of Working Group I To the Fifth Assessment Report of the Intergovernmental Panel on Climate Change (1029–1136). Cambridge University Press.

Costoya, X., DeCastro, M., Carvalho, D., Gómez-Gesteira, M., 2020b. On the suitability of offshore wind energy resource in the United States of America for the 21st century. Appl. Energy 262, 114537. http://dx.doi.org/10.1016/j.apenergy.2020.114537.

Costoya, X., DeCastro, M., Santos, F., Sousa, M.C., Gómez-Gesteira, M., 2019. Projections of wind energy resources in the Caribbean for the 21st century. Energy 178, 356–367. http://dx.doi.org/10.1016/j.energy.2019.04.121.

Costoya, X., Rocha, A., Carvalho, D., 2020a. Using bias-correction to improve future projections of offshore wind energy resource: A case study on the Iberian Peninsula. Appl. Energy 262, 114562. http://dx.doi.org/10.1016/j.apenergy.2020.114562.

Danabasoglu, G., Lamarque, J.F., Bacmeister, J., Bailey, D.A., DuVivier, A.K., Edwards, J., et al., 2020. The community earth system model version 2 (CESM2). J. Adv. Model. Earth Syst. 12, e2019MS001916. http://dx.doi.org/10.1029/2019MS001916.

deCastro, M., Salvador, S., Gómez-Gesteira, M., Costoya, X., Carvalho, D., Sanz-Larruga, F.J., Gimeno, L., 2019. Europe, China and the United States: Three different approaches to the development of offshore wind energy. Renew. Sust. Energ. Rev. 109, 55–70. http://dx.doi.org/10.1016/j.rser.2019.04.025.

Enfield, D.B., Alfaro, E.J., 1999. The dependence of Caribbean rainfall on the interaction of the tropical Atlantic and Pacific Oceans. J. Clim. 12, 2093–2103. http://dx.doi.org/10.1175/1520-04421999.012<2093:TDOCRO>2.0.CO;2.

Eyring, V., Bony, S., Meehl, G.A., Senior, C.A., Stevens, B., Stouffer, R.J., Taylor, K.E., 2016. Overview of the Coupled Model Intercomparison Project Phase 6 (CMIP6) experimental design and organization. Geosci. Model Dev. 9, 1937–1958. http://dx.doi.org/10.5194/gmd-9-1937-2016.

Fant, C., Schlosser, C.A., Strzepek, K., 2016. The impact of climate change on wind and solar resources in southern africa. Appl. Energy 161, 556–564. http://dx.doi.org/10.1016/j.apenergy.2015.03.042.

Gallagher, S., Gleeson, E., Tiron, R., McGrath, R., Dias, F., 2016. Twenty-first century wave climate projections for Ireland and surface winds in the North Atlantic Ocean. Adv. Sci. Res. 13, 75–80. http://dx.doi.org/10.5194/asr-13-75-2016.

González, A., Pérez, J.C., Díaz, J.P., Expósito, F.J., 2017. Future projections of wind resource in a mountainous archipelago, Canary Islands. Renew. Energy 104, 120–128. http://dx.doi.org/10.1016/j.renene.2016.12.021.

GWEC, 2021. Global offshore wind report 2020. Global wind energy council. https://gwec.net/global-offshore-wind-report-2021/ Accessed 12 2021.

Hersbach, H., Bell, B., Berrisford, P., Hirahara, S., Horányi, A., J., Muñoz-Sabater, et al., 2020. The ERA5 global reanalysis. Q. J. R. Meteorol. Soc. 146, 1999–2049. http://dx.doi.org/10.1002/qj.3803.

Hong, S.Y., Lim, JOJ., 2006. The WRF single-moment 6-class microphysics scheme (WSM6). J. Meteorol. Soc. Japan 42, 129–151. http://dx.doi.org/10.1155/2010/707253.

Hong, S.Y., Noh, Y., Dudhia, J., 2006. A new vertical diffusion package with an explicit treatment of entrainment processes. Mon. Weather Rev. 134, 2318–2341. http://dx.doi.org/10.1175/MWR3199.1.

Iacono, M.J., Delamere, J.S., Mlawer, E.J., Shephard, M.W., Clough, S.A., Collins, W.D., 2008. Radiative forcing by long–lived greenhouse gases: Calculations with the AER radiative transfer models. J. Geophys. Res. 113, D13103. http://dx.doi.org/10.1029/2008JD009944.

Insua-Castro, D., Miguez-Macho, G., 2018. A new moisture tagging capability in the Weather Research and Forecasting model: formulation, validation and application to the 2014 Great lake-effect snowstorm. Earth Syst. Dyn. 9, 167–185. http://dx.doi.org/10.5194/esd-9-167-2018.

Insua-Castro, D., Miguez-Macho, G., Llasat, M.C., 2019. Local and remote moisture sources for extreme precipitation: a study of the two catastrophic 1982 western Mediterranean episodes. Hydrol. Earth Syst. Sci. 23, 3885–3900. http://dx.doi.org/10.5194/hess-23-3885-2019.

IPCC, 2021. Climate change 2021: The physical science basis. In: Contribution of Working Group I To the Sixth Assessment Report of the Intergovernmental Panel on Climate Change. Cambridge University Press, In Press.

Jimenez, P.A., Dudhia, J., Gonzalez-Rouco, J.F., Navarro, J., Montavez, J.P., Garcia-Bustamante, E., 2012. A revised scheme for the WRF surface layer formulation. Mon. Weather Rev. 140, 898–918. http://dx.doi.org/10.1175/MWR-D-11-00056.1.

Johnson, D.L., Erhardt, R.J., 2016. Projected impacts of climate change on wind energy density in the United States. Renew. Energy 85, 66–73. http://dx.doi.org/10.1016/j.renene.2015.06.005.

Kain, J.S., 2004. The Kain–Fritsch convective parameterization: An update. J. Appl. Meteorol. 43, 170–181. http://dx.doi.org/10.1175/1520-04502004.043<0170:TKCPAU>2.0.CO;2.

Kalverla, P.C., Duncan, Jr., J.B., Steeneveld, G.J., Holtslag, A.A.M., 2019. Low-level jets over the North Sea based on ERA5 and observations: together they do better. Wind Energy Sci. 4, 193–209. http://dx.doi.org/10.5194/wes-4-193-2019.

Kulkarni, S., Huang, H.P., 2014. Changes in surface wind speed over North America from CMIP5 model projections and implications for wind energy. Adv. Meteorol. 2014.

Liu, B., Costa, K.B., Xie, L., Semazzi, F.H., 2014. Dynamical downscaling of climate change impacts on wind energy resources in the contiguous United States by using a limited-area model with scale-selective data assimilation. Adv. Meteorol. 2014, http://dx.doi.org/10.1155/2014/897246.

Martinez, A., Iglesias, G., 2021. Wind resource evolution in Europe under different scenarios of climate change characterised by the novel Shared Socioeconomic Pathways. Energy Convers. Manage. 234, 113961. http://dx.doi.org/10.1016/j.enconman.2021.113961.

Miguez-Macho, G., Stenchikov, G.L., Robock, A., 2004. Spectral nudging to eliminate the effects of domain position and geometry in regional climate model simulations. J. Geophys. Res.: Atmos. 109, 1–15. http://dx.doi.org/10.1029/2003JD004495.

Moemken, J., Reyers, M., Feldmann, H., Pinto, J.G., 2018. Future changes of wind speed and wind energy potentials in EURO-CORDEX ensemble simulations. J. Geophys. Res. Atmos. 123, 6373–6389. http://dx.doi.org/10.1029/2018JD028473.

Musial, W., Heimiller, D., Beiter, P., Scott, G., Draxl, C., 2016. Offshore Wind Energy Resource Assessment for the United States. Technical Report, NREL/TP-5000-66599, National Renewable Energy Laboratory.

Nolan, D.S., Rappin, E.D., 2008. Increased sensitivity of tropical cyclogenesis to wind shear in higher SST environments. Geophys. Res. Lett. 35, 148–165. http://dx.doi.org/10.1029/2008GL034147.

Olauson, J., 2018. ERA5: The new champion of wind power modelling? Renew. Energy 126, 322–331. http://dx.doi.org/10.1016/j.renene.2018.03.056.

O'Neill, B.C., et al., 2016. The scenario model intercomparison project (scenariomip) for CMIP6. Geosci. Model Dev. 9, 3461–3482. http://dx.doi.org/10.5194/gmd-9-3461-2016.

Pryor, S.C., Schoof, J.T., Barthelmie, R.J., 2006. Winds of change? Projections of near-surface winds under climate change scenarios. Geophys. Res. Lett. 33, L11702. http://dx.doi.org/10.1029/2006GL026000.

Ramírez, L., Brindley, G., Fraile, D., 2021. Offshore wind in Europe: Key trends and statistics 2020. https://windeurope.org/intelligence-platform/product/offshore-wind-in-europe-key-trends-and-statistics-2020/. Accessed 21 2021.

Renault, L., McWilliams, J.C., Masson, S., 2017. Satellite observations of imprint of oceanic current on wind stress by air-sea coupling. Sci. Rep. 7, 17747. http://dx.doi.org/10.1038/s41598-017-17939-1.

Riahi, K., Van Vuuren, D.P., Kriegler, E., Edmonds, J., O'neill, B.C., Fujimori, S., Bauer, N., Calvin, K., Dellink, R., Fricko, O., 2017. The shared socioeconomic pathways and their energy, land use, and greenhouse gas emissions

implications: an overview. Glob. Environ. Change 42, 153–168. http://dx.doi.org/10.1016/j.gloenvcha.2016.05.009.
Ruosteenoja, K., Vihma, T., Venäläinen, A., 2019. Projected changes in European and North Atlantic seasonal wind climate derived from CMIP5 simulations. J. Clim 32, 6467–6490. http://dx.doi.org/10.1175/JCLI-D-19-0023.s1.
Salvador, S., Costoya, X., Sanz-Larruga, F.J., Gimeno, L., 2018. Development of offshore wind power: Contrasting optimal wind sites with legal restrictions in Galicia, Spain. Energies 11, 731. http://dx.doi.org/10.3390/en11040731.
Santos, F., Gómez-Gesteira, M., Añel, J.A., Carvalho, D., Costoya, X., Dias, J.M., 2018. On the accuracy of CORDEX RCMs to project future winds over the Iberian Peninsula and surrounding ocean. Appl. Energy 228, 289–300. http://dx.doi.org/10.1016/j.apenergy.2018.06.08608.
Shen, C., Zha, J., Li, Z., Molina, C.Azorin., Deng, K., Minola, L., Chen, D., 2022. Evaluation of global terrestrial near-surface wind speed simulated by CMIP6 models and their future projections. Ann. New York Acad. Sci. http://dx.doi.org/10.1111/nyas.14910.
Simpson, I.R., et al., 2020. An evaluation of the large-scale atmospheric circulation and its variability in CESM2 and other CMIP models. Geophys. Res. Atmos. 125, e2020JD032835. http://dx.doi.org/10.1029/2020JD032835.
Skamarock, W., Klemp, J., Dudhi, J., Gill, D., Barker, D., Duda, M., Huang, X., Wang, W., Powers, J., 2008. A Description of the Advanced Research WRF Version 3. Technical Report, 113, http://dx.doi.org/10.5065/D6DZ069T.
Soares, P.M., Lima, D.C., Cardoso, R.M., Nascimento, M.L., Semedo, A., 2017. Western Iberian offshore wind resources: More or less in a global warming climate? Appl. Energy 203, 72–90. http://dx.doi.org/10.1016/j.apenergy.2017.06.004.
Stocker, T.F., Dahe, Q., Plattner, G.-K., 2013. Climate change 2013: the physical science basis. Work. Group Contrib. Fifth Assess. Rep. Intergov. Panel Clim. Change Summ. Policymakers IPCC 2013.
Swart, R., Coppens, C., Gordijn, H., Piek, M., Ruyssenaars, P., Schrander, J., Smet, P.D., Hoogwijk, M., Papalexandrou, M., deVisser, E., et al., 2009. Europe's Onshore and Offshore Wind Energy Potential: An Assessment of Environmental and Economic Constraints. (No. 6/2009). European Environment Agency.
Tewari, M., Chen, F., Wang, W., Dudhia, J., LeMone, M., Mitchell, K., et al., 2004. Implementation and verification of the unified noah land surface model in the WRF model. In: 20th Conference on Weather Analysis and Forecasting/16th Conference on Numerical Weather Prediction. Seattle, WA.
Ulazia, A., Nafarrate, A., Ibarra-Berastegi, G., Sáenz, J., Carreno-Madinabeitia, S., 2019. The consequences of air density variations over northeastern scotland for offshore wind energy potential. Energies 12, 2635. http://dx.doi.org/10.3390/en12132635.
Vecchi, G.A., Soden, B.J., 2007. Increased tropical atlantic wind shear in model projections of global warming. Geophys. Res. Lett. 34, 87–102. http://dx.doi.org/10.1029/2006GL028905.
Wang, R., Liu, B., Li, H., et al., 2017. Variation of strong dust storms events in northern China during 1978–2007. Atmos. Res. 183, 166–172. http://dx.doi.org/10.1016/j.atmosres.2016.09.002.
Wright, R.M., 2001. Wind energy development in the Caribbean. Renew. Energy 24, 439–444. http://dx.doi.org/10.1016/j.renene.2018.05.090.
Yamada, T., Mellor, G., 1975. A simulation of the Wangara atmospheric boundary layer data. J. Atmos. Sci. 32, 2309–2329. http://dx.doi.org/10.1175/1520-04691975.032<2309:ASOTWA>2.0.CO;2.
Yao, Z., Xue, Z., He, R., Bao, X., Song, J., 2016. Statistical downscaling of IPCC sea surface wind and wind energy predictions for US east coastal ocean, Gulf of Mexico and Caribbean Sea. J. Ocean Univ. China 15, 577e82. http://dx.doi.org/10.1007/s11802-016-2869-0.
Zheng, C.W., 2018. Wind energy evaluation of the 21st Century MaritimeSilk Road. J. Harbin Eng. Univ. 39 (1), 16–22.
Zheng, C.W., Li, X.Y., Luo, X., Chen, X., Qian, Y.H., Zhang, Z.H., Chen …, Y.G., 2019. Projection of future global offshore wind energy resources using CMIP data. Atmos. - Ocean 57 (2), 134–148. http://dx.doi.org/10.1080/07055900.2019.1624497.
Zheng, C.W., Pan, J., 2014. Assessment of the global ocean wind energyresource. Renew. Sustain. Energy Rev. 33, 382–391.
Zheng, C.W., Pan, J., Li, C.Y., 2016. Global oceanic wind speed trends. Ocean Coast. Manag. 129, 15–24. http://dx.doi.org/10.1016/j.ocecoaman.2016.05.001.
Zheng, C.W., et al., 2022. A positive climatic trend in the global offshore wind power. Front. Energy Res. 10, 867642. http://dx.doi.org/10.3389/fenrg.2022.867642.